

Electrical field control magnetic phase transition in nanostructured $\text{Mn}_x\text{Ge}_{1-x}$

Jingjing Chen, Kang L. Wang, and Kosmas Galatsis^{a)}

Electrical Engineering Department, University of California, Los Angeles, California, 90095

(Received 28 September 2006; accepted 28 November 2006; published online 2 January 2007)

The authors have investigated the magnetic, electrical, and structural properties of $\text{Mn}_x\text{Ge}_{1-x}$ (on Ge substrate) nanostructured films produced by a nanopattern assisted Mn implantation followed by annealing. The semiconducting property and hole-mediated ferromagnetism mechanism enabled them to control the magnetic phase transition in the diluted magnetic semiconductor channel by a gate bias. © 2007 American Institute of Physics. [DOI: 10.1063/1.2424658]

Diluted magnetic semiconductor (DMS) materials have attracted a great deal of interest in recent years as they promise the possibility of combining the advantage of semiconductor band gap engineering with controllable magnetic properties in a single semiconductor device.¹ The most well accepted theory for Mn-based DMS is hole-mediated ferromagnetism²⁻⁵ based on the Ruderman-Kittel-Kasuya-Yosida (RKKY) theory. A particularly exciting development is the recent realization of ferromagnetism in Mn-doped group IV, having the compatibility with current Si-based technology and expected high Curie temperature.⁶⁻⁸

To investigate the carrier-spin exchange interactions in nanostructured films, structural control of nanostructured films is essential, since the exchange interactions are supposed to be very sensitive to atomic scale structure. In this letter, we present the study of structural, electrical, and magnetic properties in a nanostructured $\text{Mn}_x\text{Ge}_{1-x}$ DMS system with an average Mn concentration of about 2%.

We fabricated a periodic nanostructure based on $\text{Mn}_x\text{Ge}_{1-x}$ by Mn implantation into Ge (111) using a pattern as a mask. A 60 nm thick SiO_2 film was deposited on the *p*- and *n*-type (10^{19} cm^{-3} for *p*-type and 10^{17} cm^{-3} for *n*-type) Ge substrates by plasma enhanced chemical vapor deposition, followed by spinning a layer of poly(methylmethacrylate-styrene) diblock copolymer. Under a specific condition, this diblock copolymer layer forms a 20 nm scale periodic nanohole pattern on top of SiO_2/Ge substrate. After several process steps including ultra violet light and reactive ion etching, the pattern with a periodic 20 nm diameter hole structure was transferred to the SiO_2 film to form a mask. This mask was used to direct the implantation of Mn ion with 40 keV energy and a fluence of $4 \times 10^{15} \text{ cm}^{-2}$. Following implantation, rapid thermal annealing was performed on samples at 450 °C (which is an optimum annealing condition as obtained by a series of systematic experiments) in N_2 atmosphere for 20 min. During the annealing, a blank Ge wafer was capped on top of the implant samples to avoid oxidation and other contamination. The SiO_2 mask was removed by diluted hydrofluoric acid of which the samples were then annealed. After the fabrication of the DMS layer, we proceeded to fabricate a spin gated structure [i.e., metal-oxide-semiconductor (MOS) structure] using atomic layer deposition to grow a 20 nm Al_2O_3 and metallization with 400 nm Al.

Figure 1(a) shows a scanning electron microscopy (SEM) image of the SiO_2 pattern on Ge after etching and removing the diblock copolymer layer, indicating a regular and repeatable nanohole pattern with a diameter of about 20 nm. The SiO_2 pattern works as a mask for the subsequent uniform implantation of Mn into Ge. Figure 1(b) shows the uniform and smooth surface after removal of the SiO_2 . The planar transmission electron microscope (TEM) picture, shown in Fig. 1(c), shows that the $\text{Mn}_x\text{Ge}_{1-x}$ DMS nanostructure is coherently incorporated in the Ge matrix with an average Mn concentration of about 2%. The inset is the enlarged image of the DMS nanodots. The cross-section image in Fig. 1(d) shows the detailed structure of a DMS nanodot. The well resolved lattice planes extending throughout the whole image [Fig. 1(d)] reflect the high crystallinity of the layer. We can see the dot sets in a well defined distance and range from the interface [Fig. 1(d)]. A further analysis suggests that some Mn rich phase such as Mn_5Ge_3 was formed in this confined Mn implanted region, where some Mn is presumably to have been accumulated. By calculating the plane distance and angle, we discover other phases in addition to the Mn_5Ge_3 . Since the Mn concentration is about 2%, some other phases are more dilute $\text{Mn}_x\text{Ge}_{1-x}$ ($x < 5\%$) DMS phases, e.g., Mn substitutionals in Ge.

Figure 2(a) and 2(b) show the x-ray diffraction (XRD) spectra of samples annealed at a temperature of 450 °C. The XRD spectra for both *p*-type and *n*-type substrates are similar, containing stoichiometric MnGe phases with a dominant Mn_5Ge_3 phase and a negligible $\text{Mn}_{11}\text{Ge}_8$ phase. These phases have been known to possess a theoretical T_C near room temperature.^{9,10} Also, as we can see from the results, no Mn peak is seen, indicating the absence of Mn clusters. The TEM and x-ray data both show that there is a phase separation of Mn rich phases (Mn_5Ge_3 and $\text{Mn}_{11}\text{Ge}_8$) from a nanocrystalline $\text{Mn}_x\text{Ge}_{1-x}$ and Ge matrix. Though the XRD spectra of *p*- and *n*-type Ge substrate samples are similar, they exhibit different magnetic properties. As shown in Figs. 2(c) and 2(d), the Mn implanted Ge *p*-type (10^{19} cm^{-3}) sample shows a prominent ferromagnetic hysteresis loop, with T_C about 340 K, as shown in the inset; while the Mn implanted *n* type (10^{17} cm^{-3}) Ge substrate exhibits a magnetization curve without hysteresis, characteristic of a paramagnetic state. This behavior further suggests that the ferromagnetic exchange coupling in our samples is hole mediated. Since our samples have a periodic Mn-doped nanopattern, the TEM and XRD reveal a hybrid system, consisting of

^{a)}Electronic mail: kos@ee.ucla.edu

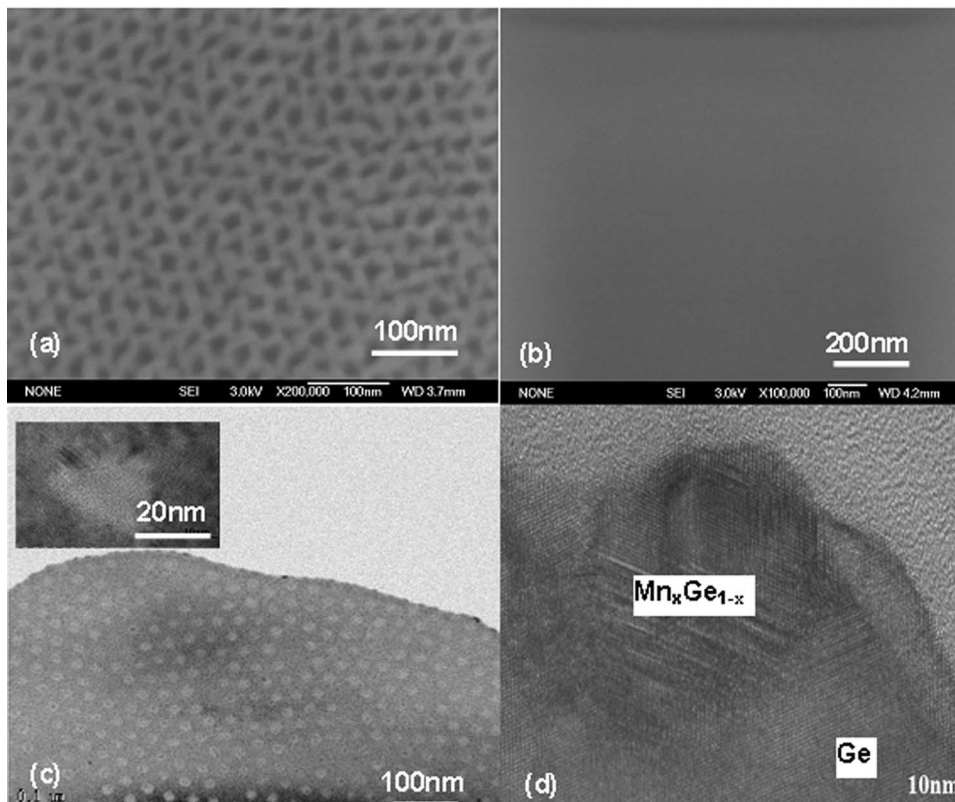


FIG. 1. SEM and TEM micrographs: (a) SEM of the periodic SiO_2 nanostructure mask before Mn implantation showing a regular and repeatable nanohole pattern with a diameter of about 20 nm. (b) SEM of sample's smooth surface after Mn implantation and removal of the SiO_2 mask. (c) TEM planar view of nanostructured $\text{Mn}_x\text{Ge}_{1-x}$ DMS. The inset figure shows enlarged dot planar view with a diameter about 20 nm. (d) TEM cross section of the nanostructured $\text{Mn}_x\text{Ge}_{1-x}$ DMS.

$\text{Mn}_x\text{Ge}_{1-x}$ DMS nanostructure (including Mn rich phase and Mn substituted in Ge) and pure Ge. According to Morresi *et al.*, the spin of localized carriers can polarize the surrounding magnetic impurities, leading to so-called bound magnetic polarons.¹¹ We consider a $\text{Mn}_x\text{Ge}_{1-x}$ nanodot as a big polaron. The alignment of the polarization is mediated by the holes in the system via interaction according to the RKKY theory.⁵

With a patterned metal layer being an Ohmic contact to the MnGe layer, we measured the resistivity versus temperature for the *n*-type sample, as shown in Fig. 3(a). The resistivity decreases with increasing temperature over the measured temperature region, suggesting that the material (DMS

and the Ge substrate) has a semiconducting characteristic. Although this is an average result of the DMS and the Ge substrate, it confirms that the material does not possess a dependence of electrical conductivity on temperature, which is typical for metals. The inset gives the linear fit of the Arrhenius plot at high temperatures, from which the activation energy $E_a \approx 0.4$ eV was obtained. This result is very consistent with the absorption data we obtained from Fourier transform infrared. Considering that pure Ge has a band gap of 0.66 eV, a model to explain sample's higher band gap compared to Ge is still required. With the fabricated MOS structure of 1 mm in diameter, we obtain the *C-V* (capacitance-voltage) curve for the *n*-type sample at

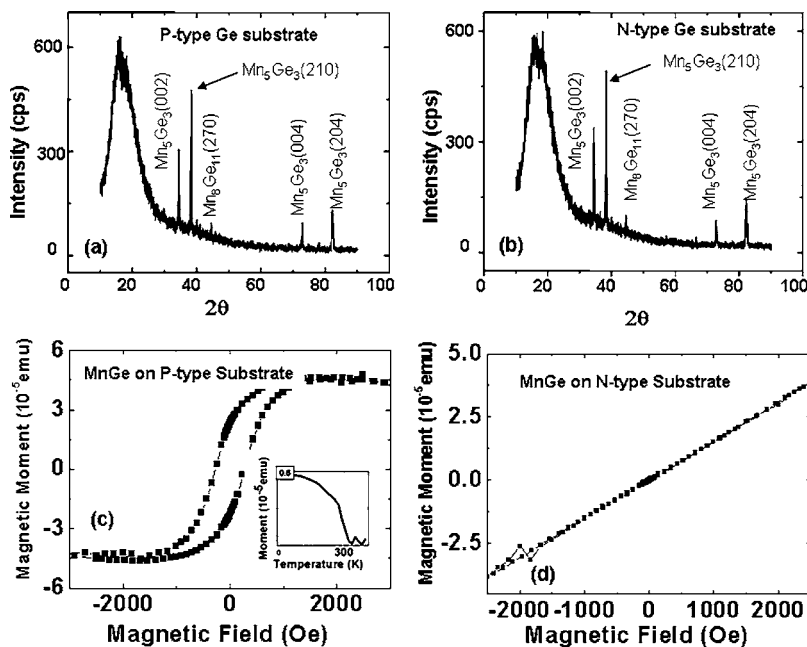


FIG. 2. XRD and superconducting quantum interference device (SQUID) results for DMS samples annealed at 450°C on *p*-type and *n*-type Ge substrates. (a) XRD result for the *p*-type DMS sample, (b) XRD result for the *n*-type DMS sample. The structures for both *p*-type and *n*-type substrates are very similar, containing stoichiometric MnGe phases with a dominant Mn_5Ge_3 phase and a negligible $\text{Mn}_{11}\text{Ge}_8$ phase. (c) SQUID result for the *p*-type DMS sample showing ferromagnetic hysteresis. The inset shows a Curie temperature above room temperature. (d) SQUID result for *n*-type DMS sample exhibiting only a paramagnetic property.

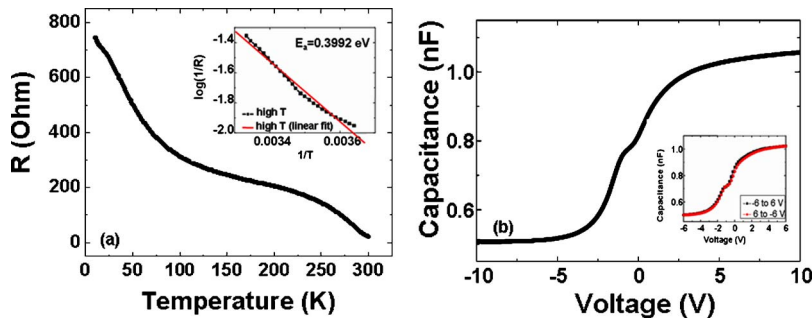


FIG. 3. (a) Temperature dependent resistivity for the *n*-type Ge substrate sample. The inset figure shows the linear fit of the Arrhenius plot at high temperature with the active energy of about 0.4 eV. (b) *C*-*V* curve of the *n*-type substrate DMS MOS structure. The inset shows a negligible hysteresis loop.

100 kHz, as shown in Fig. 3(b), with a gate bias ranging from -10 to 10 V. We can see the clear accumulation and inversion, which indicate that the surface potential and the surface carrier concentration are controlled by the applied electric field. The inset of Fig. 3(b) shows negligible hysteresis in *C*-*V*. But there is a small kink at the depletion region, which may be due to the interface traps. The relatively small flatband shift suggests the reliable gate oxide.

Figure 4 shows the magnetic moment versus applied field under various gate biases at 10 K for the DMS MOS structure on the *n*-type substrate shown in the inset. When the voltage is applied from -6 to -30 V going into strong inversion, the hole concentration increases, the magnetic hysteresis becomes larger, and the channel magnetization increases. At 0 V bias, there are still some excess holes after compensating with defects, and thus only a line with a small slope and a small negligible loop is seen. However, when a positive voltage is applied to the gate, holes are partially depleted, resulting in a decrease of the channel magnetiza-

tion and in the disappearance of magnetic hysteresis.

In summary, we reported the formation of DMS $\text{Mn}_x\text{Ge}_{1-x}$ nanostructure in Ge substrate using Mn ion implantation through a nanodot mask followed by thermal annealing treatment. TEM and XRD studies indicated the presence of Mn_5Ge_3 ferromagnetic phase. The semiconducting properties and hole-mediated exchange permit control of ferromagnetic ordering through controlling the hole concentration. The our T_C we obtained is higher than the predicted T_C calculated from the spin interaction and percolation theory.⁴ We realized a magnetic phase transition by controlling the carrier concentration in the DMS channel through gate bias in our ultimate goal to implement a spin field-effect transistor device.¹²

The authors acknowledge the MARCO Focus Center on Functional Engineered Nano Architectonics (FENA) and Mao-Nan Chang of NDL, Taiwan for support with TEM.

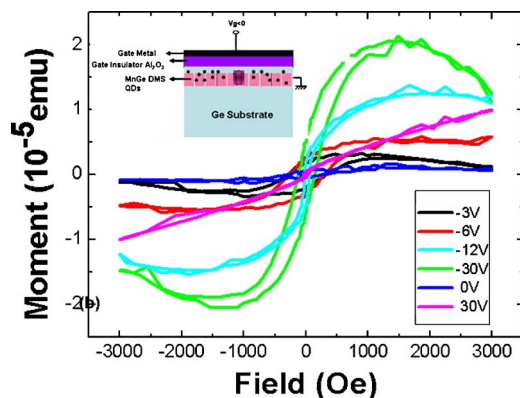


FIG. 4. Magnetic moment vs applied field under various biases from -30 to 30 V at 10 K. The obtained hysteresis is the largest under -30 V gate voltage, and the ferromagnetic phase is turned off under $+30$ V gate bias. The inset shows the spin gated structure used to investigate *C*-*V* and gate bias dependent magnetic properties.

¹T. Dietl, *Semicond. Sci. Technol.* **17**, 377 (2002).

²T. Dietl, H. Ohno, and F. Matsukura, *Phys. Rev. B* **63**, 195205 (2001).

³V. I. Litvinov and N. K. Dugaev, *Phys. Rev. Lett.* **86**, 5593 (2001).

⁴Y. D. Park, A. T. Hanbicki, S. C. Erwin, C. S. Hellberg, J. M. Sullivan, J. E. Mattson, T. F. Ambrose, A. Wilson, G. Spanos, and B. T. Jonker, *Science* **295**, 651 (2002).

⁵Z. Yu-Jun, T. Shishidou, and A. J. Freeman, *Phys. Rev. Lett.* **90**, 047204 (2003).

⁶C. Sunglae, C. Sungyool, H. Soon Cheol, K. Yunki, J. B. Ketterson, K. Bong-Jun Kim, Y. C. Kim, and J. Jung-Hyun, *Phys. Rev. B* **66**, 033303 (2002).

⁷F. D'Orazio, F. Lucari, M. Passacantando, P. Picozzi, S. Santucci, and A. Verna, *IEEE Trans. Magn.* **38**, 2856 (2002).

⁸Y. D. Park, A. Wilson, A. T. Hanbicki, J. E. Mattson, T. Ambrose, G. Spanos, B. T. Tonker, *Appl. Phys. Lett.* **78**, 2739 (2001).

⁹K. Kanematsu, *J. Phys. Soc. Jpn.* **17**, 85 (1962).

¹⁰N. Yamada, K. Maeda, Y. Usami, and T. Ohoyama, *J. Phys. Soc. Jpn.* **55**, 3721 (1986).

¹¹L. Morresi, N. Pinto, M. Ficcadenti, R. Murri, F. D'Orazio, and F. Lucari, *Mater. Sci. Eng., B* **126**, 197 (2006).

¹²D. E. Nikonov and G. I. Bourianoff, *IEEE Trans. Nanotechnol.* **4**, 206 (2005).